The synthesis and characterization of a new diphosphine-protected gold hydride nanocluster

View Online   Export Citation   CrossMark

Jia Dong, [ID] Ze-Hua Gao, and Lai-Sheng Wang[a] [ID]

AFFILIATIONS

Department of Chemistry, Brown University, Providence, Rhode Island 02912, USA

Note: This paper is part of the JCP Special Topic on From Atom-Precise Nanoclusters to Superatom Materials.
[a]Author to whom correspondence should be addressed: Lai-Sheng_Wang@brown.edu

ABSTRACT

Gold is the most inert metal and does not form a bulk hydride. However, gold becomes chemically active in the nanometer scale and gold nanoparticles have been found to exhibit important catalytic properties. Here, we report the synthesis and characterization of a highly stable ligand-protected gold hydride nanocluster, $[Au_{22}H_3(dppee)_7]^{3+}$ [dppee = bis(2-diphenylphosphino) ethyl ether]. A synthetic method is developed to obtain high purity samples of the gold trihydride nanocluster with good yields. The properties of the new hydride cluster are characterized with different experimental techniques, as well as theoretical calculations. Solid samples of $[Au_{22}H_3(dppee)_7]^{3+}$ are found to be stable under ambient conditions. Both experimental evidence and theoretical evidence suggest that the $Au_{22}H_3$ core of the $[Au_{22}H_3(dppee)_7]^{3+}$ hydride nanocluster consists of two Au_{11} units bonded via two triangular faces, creating six uncoordinated Au sites at the interface. The three H atoms bridge the six uncoordinated Au atoms at the interface. The Au_{11} unit behaves as an eight-electron trivalent superatom, forming a superatom triple bond ($Au_{11} \equiv Au_{11}$) in the $[Au_{22}H_3(dppee)_7]^{3+}$ trihydride nanocluster assisted by the three bridging H atoms.

Published under an exclusive license by AIP Publishing. https://doi.org/10.1063/5.0056958

I. INTRODUCTION

The discovery of catalytic effects by gold nanoparticles[1,2] has stimulated significant research interest into the structures and properties of gaseous size-selected gold clusters.[3–7] These clusters with well-defined size and structures can serve as ideal models to elucidate the catalytic mechanisms of gold nanoparticles.[8–10] One particularly interesting gold cluster is the tetrahedral Au_{20}, which is found to possess a highly symmetric pyramidal structure with all atoms on the cluster surface.[11] The pyramidal structure of Au_{20} has been confirmed by various experimental techniques,[12–16] and it has been shown to exhibit interesting chemical and optical properties.[17–19] The Au_{20} pyramid would be an ideal model catalyst with its well-defined surface sites. To harness the myriad of novel properties of the Au_{20} pyramid, it would be desirable to synthesize it in bulk quantities. The four corner sites of Au_{20} provide good sites for ligand coordination and protection, while the uncoordinated edge and face-center atoms would still be available as *in situ* catalytic active sites.[20,21]

Phosphine ligands were computationally shown to be able to coordinate to the corner sites of Au_{20} while maintaining the tetrahedral structure, which was observed in solution using electrospray ionization (ESI) mass spectrometry in an early synthetic attempt.[20] In order to increase the synthetic yield and find the optimal ligand for the Au_{20} pyramid, we investigated diphenyl ligands with different chain lengths, $PPh_2–(CH_2)_M–PPh_2$ (L^M for short), and indeed observed size-selectivity for different gold clusters (Au_n, $n < 12$) for $M = 1$–6.[22] Subsequently, we found that the L^8 ligand yielded a Au_{22} cluster protected by six ligands. A single crystal structure was obtained for the new $Au_{22}(L^8)_6$ cluster, which was found to contain two Au_{11} units bonded by a square face from each Au_{11}.[23] Most interestingly, the eight Au atoms at the interface of the two Au_{11} units in $Au_{22}(L^8)_6$ were uncoordinated and could be used as *in situ* catalytic sites. Using a bis(2-diphenylphosphino)ethyl ether [dppee, Fig. 1(a)] ligand, we were able to synthesize another novel Au_{22} cluster, $Au_{22}(dppee)_7$, showing polymorphism of diphosphine-protected gold nanoclusters.[24] Even though we were not able to obtain the crystal structure of this new $Au_{22}(dppee)_7$ cluster, we showed that it contained a Au_{11} unit on the bases of its ultraviolet and visible (UV-Vis) absorption spectrum and collision-induced dissociation (CID) experiments.

The $Au_{22}(L^8)_6$ cluster represents the first atom-precise gold nanocluster with uncoordinated surface sites, which have been demonstrated to provide excellent *in situ* active sites for CO
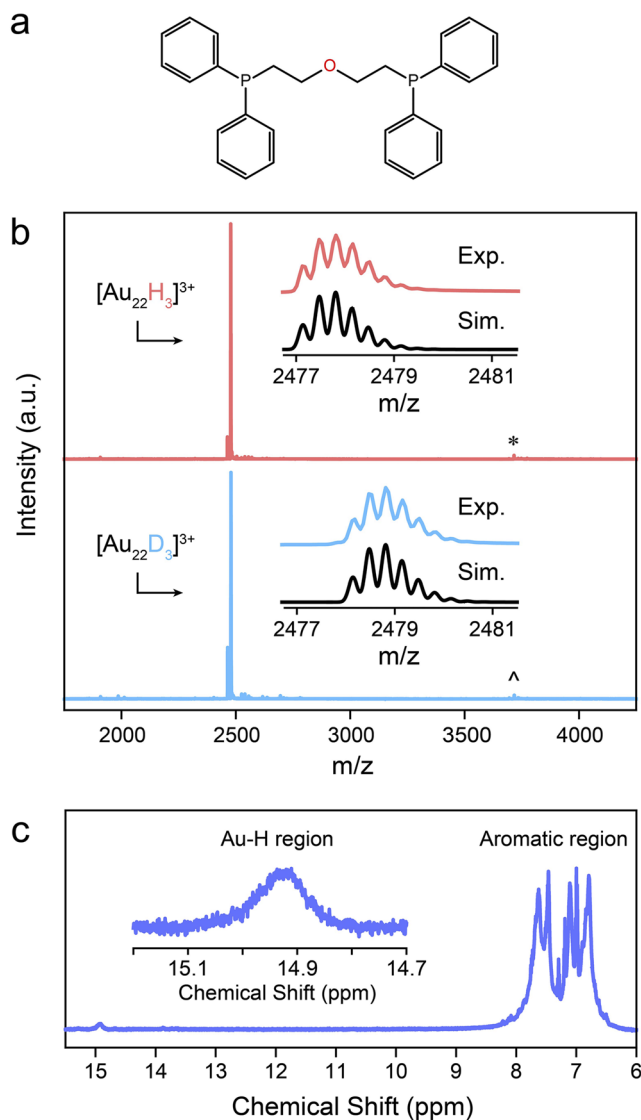
FIG. 1. Characterization of the $[Au_{22}H_3(dppee)_7]^{3+}$ hydride nanocluster. (a) The structure of the dppee ligand. (b) ESI mass spectra of $[Au_{22}H_3(dppee)_7]^{3+}$ and $[Au_{22}D_3(dppee)_7]^{3+}$; the insets show the experimental and simulated isotopic distributions. The minor peaks denoted by * and ^ are $[Au_{22}H_2(dppee)_7]^{2+}$ and $[Au_{22}D_2(dppee)_7]^{2+}$, respectively. (c) The ^1H-NMR spectrum of $[Au_{22}H_3(dppee)_7]^{3+}$; the inset shows the enlarged signal in the Au–H region.

the $[Au_{22}H_4(L^8)_6]^{2+}$ hydride nanocluster can be a versatile model catalyst for understanding reaction mechanisms involving hydrogen on the surfaces of gold nanoparticles.

Gold is the most inert metal and does not form a bulk hydride even under extreme conditions,[30,31] even though small gold clusters are known to react with H_2 to form hydride clusters.[32–35] There is also evidence of surface gold hydride formation.[36–39] Atom-precise gold nanoclusters protected by ligands have experienced a tremendous development over the past decade.[40–48] A phosphine-protected gold cluster, $[Au_9(PPh_3)_8]^{3+}$, was observed to react with $NaBH_4$ to give a metastable $[Au_9H(PPh_3)_8]^{2+}$ monohydride cluster,[49] which was investigated by nuclear magnetic resonance (NMR) spectroscopy and electronic spectroscopy.[50] Some H-containing small phosphine-gold clusters have been observed in ESI mass spectra as intermediates during gold cluster syntheses.[51–53] A stable $[Au_{20}H_3(PPh_3)_{12}]^{3+}$ hydride cluster has also recently been reported.[54] Our previous $Au_{22}(dppee)_7$ nanocluster was observed in ESI mass spectra as a protonated $[Au_{22}H_3(dppee)_7]^{3+}$ species.[24] The protonation was thought, at the time, to have taken place during the ESI process from the acidic acid that was commonly added to the ESI solution to assist ion formation. In light of our recent discovery of the $[Au_{22}H_4(L^8)_6]^{2+}$ tetrahydride gold nanocluster,[29] we revisited the $Au_{22}(dppee)_7$ nanocluster, which was synthesized by using $NaBH_4$ as the reducing agent. When we used $NaBD_4$ as the reducing agent, we observed $[Au_{22}D_3(dppee)_7]^{3+}$ in the ESI mass spectra, suggesting that the $[Au_{22}H_3(dppee)_7]^{3+}$ trihydride nanocluster was, in fact, the as-synthesized product rather than that formed during the ESI process. More importantly, we have found that the $[Au_{22}H_3(dppee)_7]^{3+}$ trihydride nanocluster is much more stable than the $[Au_{22}H_4(L^8)_6]^{2+}$ tetrahydride gold nanocluster.[29]

In this article, we report the synthesis, purification, and characterization of the new $[Au_{22}H_3(dppee)_7]^{3+}$ gold trihydride nanocluster. Even though we have not been able to obtain the single crystal structure of $[Au_{22}H_3(dppee)_7]^{3+}$, we have deduced, using a variety of experimental and theoretical methods, that the Au_{22} core consists of two Au_{11} units bonded together via two triangular faces with the three H atoms bridging the six uncoordinated Au atoms at the interface. Chemical bonding analyses reveal that the Au_{22} core consists of a $Au_{11} \equiv Au_{11}$ superatom–superatom triple bond assisted by the three bridging H atoms. The $[Au_{22}H_3(dppee)_7]^{3+}$ trihydride nanocluster can be easily prepared with a reasonable yield and is stable in the solid state at ambient conditions, opening up new opportunities to explore its catalytic properties.

II. EXPERIMENTAL AND THEORETICAL METHODS

A. Chemicals

The chemicals used in the current work included chloro (dimethylsulfide)gold(I) [ClAuS(CH_3)_2, Sigma-Aldrich], bis(2-diphenylphosphino)ethyl ether (dppee, Strem), sodium borohydride (NaBH_4, Sigma-Aldrich), sodium borodeuteride (NaBD_4, Sigma-Aldrich), methylene chloride (CH_2Cl_2, Fisher Scientific), ethanol (C_2H_5OH, Sigma-Aldrich), ethanol-OD (C_2H_5OD, Sigma-Aldrich), ethyl acetate (CH_3CO_2C_2H_5, Fisher Scientific), and methanol (CH_3OH, Fisher Scientific). All these chemicals were used directly as received.

oxidation.[25–27] More interestingly, the $Au_{22}(L^8)_6$ nanocluster was computationally found to display excellent hydrogen absorption properties for the H_2 evolution reaction because it can bind up to six hydrogen atoms at near zero adsorption free energies at ambient conditions.[28] In our effort to study the reactivity of $Au_{22}(L^8)_6$ with H_2, we recently discovered that the as-synthesized sample was, in fact, in the form of a tetrahydride, $[Au_{22}H_4(L^8)_6]^{2+}$, which lost its hydrogens during the slow crystallization process.[29] Extensive investigations uncovered its hydrogen loss mechanisms and showed that

B. Experimental characterization methods

UV-Vis absorption spectra were measured at room temperature on a Varian Cary 50 Bio spectrometer with a spectral range between 300 and 800 nm. The ^{1}H, ^{2}H, ^{31}P-NMR spectra were obtained on a 600 MHz Bruker Ultrashield spectrometer using CD_2Cl_2 as the solvent at 298 K unless further noted. Chemical shifts (δ) are reported in ppm and referenced to internal solvent resonances for ^{1}H and ^{2}H-NMR and external 85% H_3PO_4 for ^{31}P-NMR. Fourier-transform infrared (FTIR) spectra were acquired at 298 K on a Bruker Tensor 27 FTIR spectrometer with a spectral range from 400 to 4000 cm^{-1}. ESI mass spectra and CID spectra were measured on an Agilent 6530 Accurate Mass Q-TOF LC-MS system (with Agilent 1260 HPLC) and recorded at a rate of 1 spectrum s^{-1}. The CH_2Cl_2 solution of the sample (~1.0 mg ml^{-1}) was introduced into the system at a flow rate of 200 μl min^{-1}. The mobile phase was made of acetonitrile/water (50/50). The ESI source temperature was 130 °C. The fragmentor voltage was set at 50 V, the skimmer was set at 65 V, and the capillary voltage was set at +3500 V. The observed species in the ESI mass spectra were assigned by comparing the experimental and simulated isotopic distributions.

C. The syntheses of Au$_2$(dppee)Cl$_2$ and [Au$_{22}$H$_3$(dppee)$_7$]$^{3+}$

The general synthetic procedure is similar to our previous report[24] with some minor modifications. The reactions were carried out at ambient conditions in air. A 50 ml Schlenk flask was filled with 221 mg (0.50 mmol) of dppee dissolved in 2.5 ml anhydrous dichloromethane. Upon stirring, the dppee solution was quickly added with 294 mg (1.00 mmol) of ClAuS(CH$_3$)$_2$ dissolved in 11.5 ml anhydrous dichloromethane. The reaction was carried out at room temperature under dark for 48 h. After the removal of all solvents, the obtained white solid Au$_2$(dppee)Cl$_2$ was washed with pentane, dried under vacuum, and further characterized by ^{1}H and ^{31}P-NMR spectroscopy (Figs. S1 and S2). A sample of 102 mg solid Au$_2$(dppee)Cl$_2$ was further dissolved in 85 ml CH$_2$Cl$_2$, and the solution was transferred into a 200 ml Schlenk flask. After stirring the solution for over 15 min at room temperature, 3.5 ml ethanol solution of sodium borohydride (4.1 mg/ml) was quickly added into the system. The reaction was stirred for 20 h under dark at room temperature. Then, the reaction solution was dried and the remained dark brown solid was sequentially extracted with 2 × 10 ml CH$_2$Cl$_2$ and 1 ml methanol. The extracted compounds were combined, dried, and purified by silica-gel column chromatography (CH$_2$Cl$_2$/ethyl acetate/methanol = 8/2/3). Finally, a sample of 20.5 mg [Au$_{22}$H$_3$(dppee)$_7$]$^{3+}$ hydride nanocluster was obtained with a purity of >95%. If all counter anions were assumed to be chloride, the yield of [Au$_{22}$H$_3$(dppee)$_7$]$^{3+}$ was calculated to be 27% on the basis of the Au atoms.

D. Theoretical methods

Geometric optimizations and vibrational frequency calculations for all models of [Au$_{22}$H$_3$(dppee)$_7$]$^{3+}$ were performed using density functional theory (DFT) with the generalized gradient approximation (GGA)-type BPBE functional[55,56] and the 6-31G(d) basis set for C, H, P, and the LANL2DZ scalar relativistic pseudopotential basis set for Au. The phenyl rings on the dppee ligands were replaced by hydrogen to simplify the calculations. Linear-response time-dependent (TD-DFT) calculations were performed for the relaxed structures at the PBE0/6-31G(d)/LANL2DZ levels,[57] focusing on the first 600 singlet transitions. Orbital composition analyses were done using the Multiwfn 3.7 software,[58] and the chemical bonding analysis was done using the Adaptive Natural Density Partitioning (AdNDP) approach.[59] All calculations were carried out using the Gaussian 09 software package.[60]

III. RESULTS AND DISCUSSION

A. Characterization of the [Au$_{22}$H$_3$(dppee)$_7$]$^{3+}$ hydride nanocluster

The [Au$_{22}$H$_3$(dppee)$_7$]$^{3+}$ cluster was synthesized by reacting NaBH$_4$ with the Au$_2$(dppee)Cl$_2$ precursor, as described in Sec. II. After purification, the final product showed a distinct peak in the ESI mass spectrum [Fig. 1(b)] due to [Au$_{22}$H$_3$(dppee)$_7$]$^{3+}$. To confirm that the three hydrogen atoms on [Au$_{22}$H$_3$(dppee)$_7$]$^{3+}$ are part of the as-synthesized product and not coming from the ESI process, we used NaBD$_4$ instead of NaBH$_4$ to do the same reaction and obtained [Au$_{22}$D$_3$(dppee)$_7$]$^{3+}$ [Fig. 1(b)]. More importantly, the hydride was confirmed by ^{1}H-NMR, as shown in Fig. 1(c), where a small peak was observed at ~15 ppm. The ratio of the integrated area for this hydride peak to that of the 140 aromatic H atoms on the seven dppee ligands (in the range of ~6.5–8 ppm) is 3:140. This observation was also corroborated by the ^{2}H-NMR spectrum of [Au$_{22}$D$_3$(dppee)$_7$]$^{3+}$ (Fig. S3). These observed chemical shifts indicate that the three hydrogen atoms are directly bonded to Au, similar to those observed in the two previous gold hydride nanoclusters, ~15.1 ppm in the [Au$_9$H(PPh$_3$)$_8$]$^{2+}$ monohydride cluster[49] and ~15.5 ppm in the [Au$_{22}$H$_4$(L^8)$_6$]$^{2+}$ tetrahydride cluster.[29]

We have obtained highly pure [Au$_{22}$H$_3$(dppee)$_7$]$^{3+}$ nanocluster samples using column separation [Fig. 1(b)]. The high purity sample is stable in the solid state at room temperature: no decomposition was observed in the ESI mass spectrum for the sample stored for two months under ambient conditions (Fig. 2). We also found that the [Au$_{22}$H$_3$(dppee)$_7$]$^{3+}$ nanocluster is not sensitive to light or alcohol, different from the [Au$_{22}$H$_4$(L^8)$_6$]$^{2+}$ nanocluster[29]

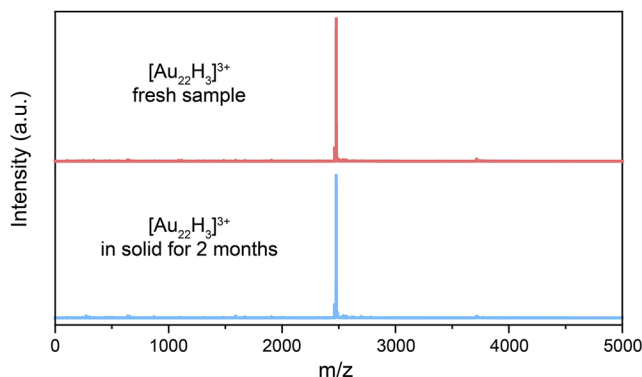**FIG. 2.** ESI mass spectra of the [Au$_{22}$H$_3$(dppee)$_7$]$^{3+}$ cluster stored in the solid form under ambient conditions after two months, showing no decomposition for the high purity nanohydride sample (bottom), compared to the fresh sample (top).

or small gold hydride intermediates reported previously.[51] When $[Au_{22}H_3(dppee)_7]^{3+}$ was dissolved in dichloromethane at room temperature, detectable decompositions were observed in the ESI mass spectrum after nine days, as shown in Fig. S4. However, the decomposition was relatively minor and almost negligible in the UV-Vis absorption spectrum (Fig. S5).

The $[Au_{22}H_3(dppee)_7]^{3+}$ trihydride nanocluster is found to be much more stable than the $[Au_{22}H_4(L^8)_6]^{2+}$ tetrahydride nanocluster. The $[Au_{22}H_4(L^8)_6]^{2+}$ cluster was shown to lose its H atoms slowly through three pathways: H evolution (H_2), proton (H^+), and hydride (H^-) releases.[29] However, $[Au_{22}H_3(dppee)_7]^{3+}$ was only observed to lose one proton during ESI, giving rise to a very weak $[Au_{22}H_2(dppee)_7]^{2+}$ signal in the mass spectra [Fig. 1(b) and Fig. S6]. When $[Au_{22}H_3(dppee)_7]^{3+}$ was heated in a dichloromethane solution, no H_2 signal was detected using ^{1}H-NMR below 75 °C, as shown in Fig. 3(a). The H_2 ^{1}H-NMR signal observed at 4.6 ppm at 75 °C is identical to that observed due to the H_2 release in the $[Au_{22}H_4(L^8)_6]^{2+}$ tetrahydride.[29] Although ethanol was found not to react with $[Au_{22}H_3(dppee)_7]^{3+}$ (Fig. S7), hydride exchange was observed when we added an ethanol solution of $NaBD_4$ to a CH_2Cl_2 solution of $[Au_{22}H_3(dppee)_7]^{3+}$. The hydride exchange reactions resulted in $[Au_{22}H_{3-x}D_x(dppee)_7]^{3+}$ species ($x = 1–3$), as shown in Fig. 3(b). Remarkably, only a very small amount of the parent $[Au_{22}H_3(dppee)_7]^{3+}$ was left after the addition of $NaBD_4$, suggesting that the hydride exchange between $[Au_{22}H_3(dppee)_7]^{3+}$ and $NaBD_4$ happens more readily than that between $[Au_{22}H_4(L^8)_6]^{2+}$ and $NaBD_4$ (Fig. S8). Adding $NaBH_4$ into a CH_2Cl_2 solution of $[Au_{22}D_3(dppee)_7]^{3+}$ led to similar isotopic scrambling (Fig. S9).

B. Structural similarity between the $[Au_{22}H_3(dppee)_7]^{3+}$ and $[Au_{22}H_4(L^8)_6]^{2+}$ hydride nanoclusters

Because single crystals of $[Au_{22}H_3(dppee)_7]^{3+}$ that we were able to grow after extensive crystallization efforts were too small to allow for x-ray diffraction experiments, we have tried to obtain structural information of the trihydride nanocluster using different

experimental techniques. We found that the trihydride nanocluster exhibits some structural similarity to that of the previously reported $[Au_{22}H_4(L^8)_6]^{2+}$ tetrahydride nanocluster.[29] Figure 4(a) compares the UV-Vis absorption spectra of $[Au_{22}H_3(dppee)_7]^{3+}$,

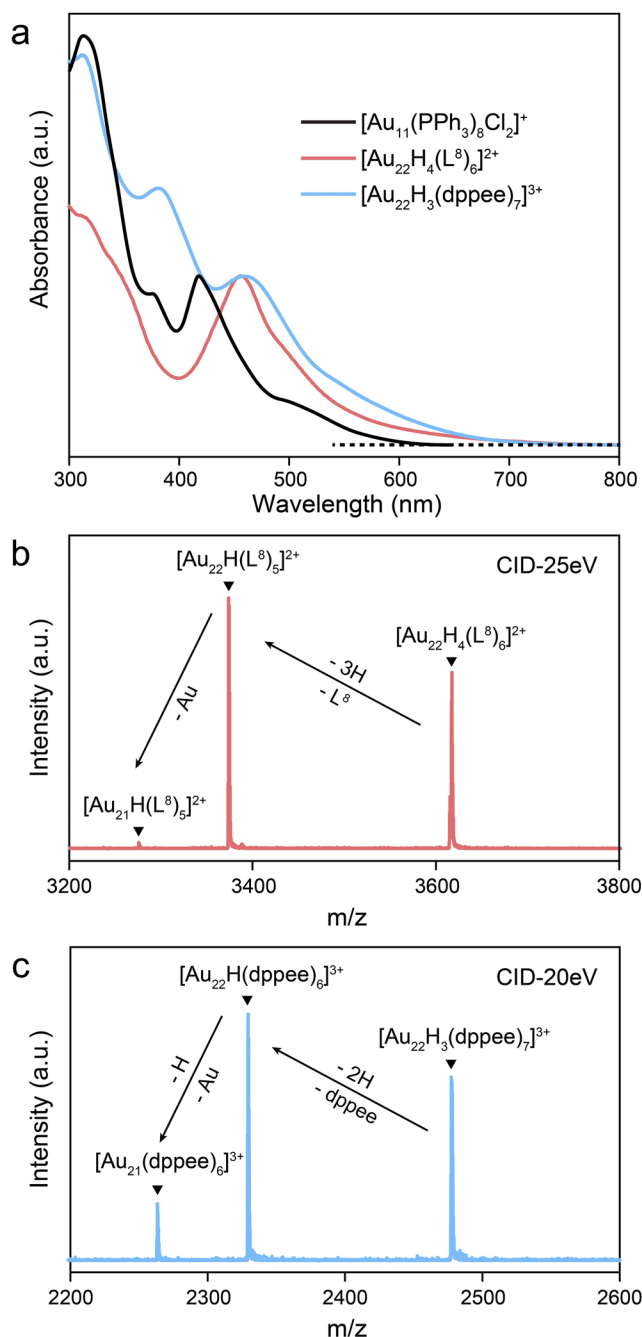**FIG. 4.** (a) Comparison of the UV-Vis absorption spectra of $[Au_{11}(PPh_3)_8Cl_2]^+$,[61] $[Au_{22}H_4(L^8)_6]^{2+}$,[29] and $[Au_{22}H_3(dppee)_7]^{3+}$. (b) The CID spectrum of $[Au_{22}H_4(L^8)_6]^{2+}$. (c) The CID spectrum of $[Au_{22}H_3(dppee)_7]^{3+}$.

FIG. 3. The H loss pathways for $[Au_{22}H_3(dppee)_7]^{3+}$. (a) Variable-temperature H_2 ^{1}H-NMR spectra from $[Au_{22}H_3(dppee)_7]^{3+}$. The H_2 signal was produced due to H···H recombination from $[Au_{22}H_3(dppee)_7]^{3+}$ at elevated temperatures (>75 °C). (b) The isotopic distribution as a result of H exchange between $[Au_{22}H_3(dppee)_7]^{3+}$ and $NaBD_4$.

$[Au_{22}H_4(L^8)_6]^{2+}$, and $[Au_{11}(PPh_3)_8Cl_2]^+$. The $[Au_{11}(PPh_3)_8Cl_2]^+$ cluster displays three major absorption peaks at 312, 380, and 416 nm.[61] Since the Au_{22} core in $[Au_{22}H_4(L^8)_6]^{2+}$ consists of two Au_{11} units bonded via eight uncoordinated gold atoms (Fig. S10), $[Au_{22}H_4(L^8)_6]^{2+}$ displays some similar absorption spectral features as the $[Au_{11}(PPh_3)_8Cl_2]^+$ cluster (Table I). Due to the increased cluster size, the 416 nm peak in $[Au_{11}(PPh_3)_8Cl_2]^+$ was red-shifted to 456 nm in $[Au_{22}H_4(L^8)_6]^{2+}$. Notably, $[Au_{22}H_3(dppee)_7]^{3+}$ also shares the same absorption spectral features as $[Au_{11}(PPh_3)_8Cl_2]^+$ and has a red-shifted peak at 459 nm. This result suggests that the Au_{22} core in $[Au_{22}H_3(dppee)_7]^{3+}$ may also be composed of two Au_{11} units bonded via gold atoms similar to that in $[Au_{22}H_4(L^8)_6]^{2+}$.

To further confirm the structural similarity between the $[Au_{22}H_3(dppee)_7]^{3+}$ and $[Au_{22}H_4(L^8)_6]^{2+}$ hydride nanoclusters, we compared their CID behaviors, as shown in Figs. 4(b) and 4(c). The major CID products of both $[Au_{22}H_3(dppee)_7]^{3+}$ and $[Au_{22}H_4(L^8)_6]^{2+}$ involved the loss of one ligand and one or two H atoms, resulting in the monohydride Au_{22} species. A minor CID product was the loss of an Au atom to form the $[Au_{21}(dppee)_6]^{3+}$ and $[Au_{21}H(L^8)_5]^{2+}$ species. The similar CID pathways for both clusters suggested that $[Au_{22}H_3(dppee)_7]^{3+}$ may have a similar Au_{22} core and ligand arrangements as the $[Au_{22}H_4(L^8)_6]^{2+}$ cluster.

The Au–H ^{1}H-NMR chemical shift [~15 ppm in Fig. 1(c)] of $[Au_{22}H_3(dppee)_7]^{3+}$ is similar to the Au–H chemical shift (~15.6 ppm) of $[Au_{22}H_4(L^8)_6]^{2+}$,[29] suggesting that the three H atoms in the new trihydride cluster are likely in bridging positions of uncoordinated Au atoms similar to that in the tetrahydride cluster (Fig. S10). The ^{31}P-NMR spectra of $[Au_{22}H_3(dppee)_7]^{3+}$ and $[Au_{22}H_4(L^8)_6]^{2+}$ displayed multiple peaks and fall in the same spectral range (45–55 ppm), as shown in Fig. S11, again consistent with their structural similarity. Interestingly, the ^{31}P-NMR spectrum of $[Au_{22}H_3(dppee)_7]^{3+}$ showed one sharp peak around 50 ppm, suggesting that the structure of $[Au_{22}H_3(dppee)_7]^{3+}$ may be more symmetrical or more rigid than $[Au_{22}H_4(L^8)_6]^{2+}$.

C. Structural models for the $[Au_{22}H_3(dppee)_7]^{3+}$ trihydride nanocluster

All the experimental evidence and comparisons with $[Au_{22}H_4(L^8)_6]^{2+}$ suggest that there are considerable similarities of the Au_{22} cores in the two gold hydride nanoclusters, both containing fused Au_{11} units, but different surface coordination sites. Hence, the $[Au_{22}H_3(dppee)_7]^{3+}$ trihydride nanocluster most likely consists of two Au_{11} units bonded via two triangular faces, as schematically shown in Fig. 5(a), giving rise to six uncoordinated Au atoms at the interface bridged by the three H atoms and 14 surface Au sites for coordination by the seven bidentate dppee ligands. More details of the $Au_{22}H_3$ core in $[Au_{22}H_3(dppee)_7]^{3+}$ are illustrated in
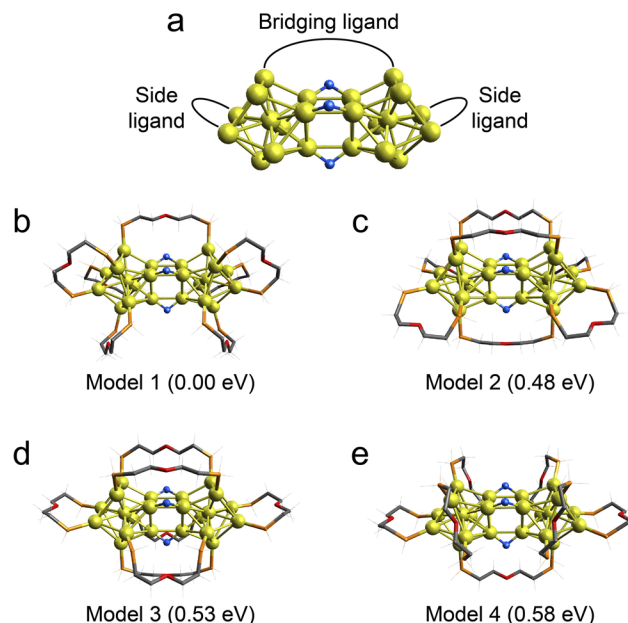
TABLE I. Comparison of the main UV-Vis absorption features of the $[Au_{11}(PPh_3)_8Cl_2]^+$, $[Au_{22}H_4(L^8)_6]^{2+}$, and $[Au_{22}H_3(dppee)_7]^{3+}$ clusters.

	Main absorption peaks (nm)		
$[Au_{11}(PPh_3)_8Cl_2]^+$ (Ref. 61)	416	380	312
$[Au_{22}H_4(L^8)_6]^{2+}$ (Ref. 29)	456	⋯	313
$[Au_{22}H_3(dppee)_7]^{3+}$	459	381	312

FIG. 5. Proposed structures for the $[Au_{22}H_3(dppee)_7]^{3+}$ cluster. (a) The proposed Au_{22} metal core with three bridging H atoms. [(b)–(e)] Optimized structures for models 1–4 of $[Au_{22}H_3(dppee)_7]^{3+}$. Colors: Au = yellow, H = blue, P = orange, and C = black. The H atoms on the ligands are depicted as gray. Relative energies are shown in the parentheses.

Fig. S12(a), which are similar to that in $[Au_{22}H_4(L^8)_6]^{2+}$, where the Au_{22} core is bonded via two square faces with eight uncoordinated Au sites bridged by four H atoms (Fig. S10) and 12 surface Au sites for coordination by the six bidentate L^8 ligands. Using DFT calculations, we examined different positions for the hydrogen atoms on the proposed Au_{22} core of $[Au_{22}H_3(dppee)_7]^{3+}$ and found that the three hydrogens are only stable to bridge the six uncoordinated gold sites of the Au_{22} cluster [Fig. 5(a) and Fig. S12(a)] similar to those in $[Au_{22}H_4(L^8)_6]^{2+}$, as expected. A similar structural behavior was also found in the $[Au_{20}(PPh_3)_{12}H_3]^{3+}$ cluster, where the Au_{20} core was composed of a Au_{11} and a Au_9 unit bonded by two triangular faces.[54]

We further considered the possible ligand arrangements in the $[Au_{22}H_3(dppee)_7]^{3+}$ cluster. In the tetrahydride cluster (Fig. S10), we found four bridging L^8 ligands linking the two Au_{11} units and one ligand coordinated to each Au_{11} in a bidentate fashion. Similarly, the seven dppee ligands can either act as a bridging ligand linking the two Au_{11} units or as a bidentate (side) ligand coordinated to a single Au_{11} unit, as schematically shown in Fig. 5(a). Because there are seven coordination sites on each Au_{11} unit, there can only be three possible bridging ligand arrangements for $[Au_{22}H_3(dppee)_7]^{3+}$, i.e., 1, 3, and 5. We optimized the structures of these ligand arrangements, as shown in Figs. 5(b)–5(e), as models 1–4. In Fig. S12, we present more details about the coordination environments for the four ligand arrangements. It turned out that there are two configurations for the case of one bridging ligand, shown as models 1 and 4, whereas models 2 and 3 contain three and five bridging ligands, respectively. All these structures were successfully optimized at the

PBE0 level of theory; their coordinates are given in Table S1. We found that model 1 with a single bridging ligand is the most stable structure, and the other three structures are higher in energy by 0.48–0.58 eV [Figs. 5(c)–5(e)].

The stability of model 1 with a single bridging ligand is somewhat surprising because we expected model 2 with three bridging ligands to be preferred on the basis of the structure of the tetrahydride, which contains four bridging L^8 ligands. The energetic advantage of model 1 is probably due to the fact that the dppee ligand is shorter than the L^8 ligand, and there may be some strains for the bridging ligands. To further assess if model 1 is the most reasonable structure for $[Au_{22}H_3(dppee)_7]^{3+}$, we simulated the absorption spectrum for each structure using TD-DFT calculations, as shown in Fig. 6. The good agreement between the experimental UV-Vis spectrum and the simulated spectrum provides further confirmation for the validity of model 1 (Fig. 6). However, the simulated UV-Vis spectra of models 2 and 3 (Fig. 6) are not too different from that of model 1 and they probably cannot be ruled out without crystallographic data. On the other hand, the simulated spectrum of model 4 is quite different (Fig. 6), and it can probably be ruled out. It should be pointed out that the sharp peak in the ^{31}P-NMR spectrum (Fig. S11) may suggest one of the dppee ligand is more rigid, providing possible support for model 1.

We were able to observe the Au–H vibrations in $[Au_{22}H_4(L^8)_6]^{2+}$ using FTIR spectroscopy.[29] We also obtained the FTIR spectrum of $[Au_{22}H_3(dppee)_7]^{3+}$ to observe the Au–H vibration, as compared with the simulated spectrum in Fig. S13. The Au–H asymmetric vibrations were computed to be around 1300 cm^{-1},

which unfortunately overlapped with the C–C vibrations of the ligands in the same spectral region (Fig. S13). However, the broad width of the observed FTIR spectrum is consistent with the presence of the Au–H vibrational feature, providing support for the three bridging H atoms. We further note that the isotope exchange reactions between $[Au_{22}H_3(dppee)_7]^{3+}$ and NaBD$_4$ seemed to take place much faster than that of $[Au_{22}H_4(L^8)_6]^{2+}$ [Fig. 3(b) and Fig. S8]. This observation also provides indirect support for model 1 because the H atoms are more accessible sterically with only one bridging ligand.

D. Chemical bonding in the $[Au_{22}H_3(dppee)_7]^{3+}$ gold trihydride nanocluster

The Au$_{22}$H$_3$ cores in all the structural models shown in Fig. 5 are similar. We analyzed the chemical bonding in the Au$_{22}$H$_3$ core for model 1 using the AdNDP method,[59] as shown in Fig. 7 and Fig. S14. The AdNDP results reveal that the three hydrogens participate in the electronic structure of the gold cluster, similar to the hydrogens found in $[Au_{22}H_4(L^8)_6]^{2+}$, $[Au_9H(PPh_3)_8]^{2+}$, $[Au_{25}H(SR)_{18}]$, and $[Au_{25}H_2(SR)_{18}]^+$,[29,49,62] but different from the hydrogens that show halide behaviors.[50] The $[Au_{22}H_3(dppee)_7]^{3+}$ cluster is found to contain 22 valence electrons. Each Au$_{11}$ unit in $[Au_{22}H_3(dppee)_7]^{3+}$ possesses eight valence electrons (Fig. S14), and the remaining six valence electrons form one superatom-σ bond and two superatom-π bonds between the two Au$_{11}$ units along with the three hydrogen atoms (Fig. 7). Therefore, each Au$_{11}$ unit can be viewed as a trivalent superatom that carries 11 valence electrons, consisting of the eight-electron superatom configuration with three unpaired electrons, forming the cluster-cluster triple bond in $[Au_{22}H_3(dppee)_7]^{3+}$. This bonding picture can be clearly seen in the full AdNDP results in Fig. S14. The superatom–superatom triple-bonding pattern is similar to that in the Au$_{22}$(L^8)$_6$ cluster[63] or the quadruple-bond in the $[Au_{22}H_4(L^8)_6]^{2+}$ cluster.[29] The formation of the superatom triple bond results in a highly stable
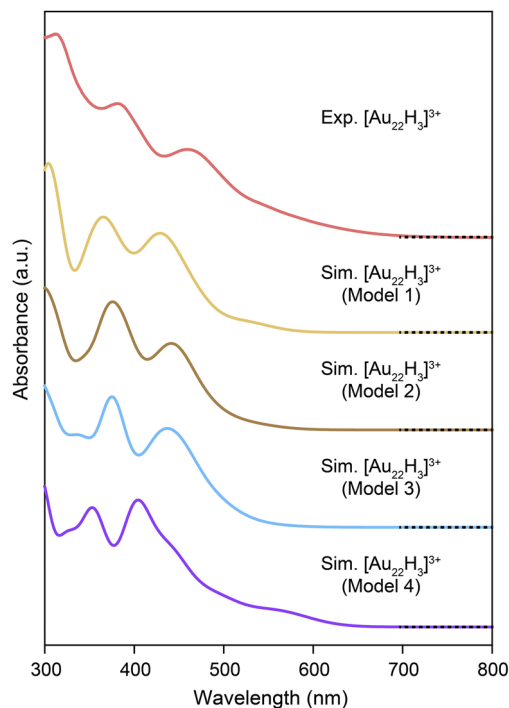

FIG. 6. Comparison between the experimental and simulated (models 1–4) UV-Vis absorption spectra of the $[Au_{22}H_3(dppee)_7]^{3+}$ nanohydride.
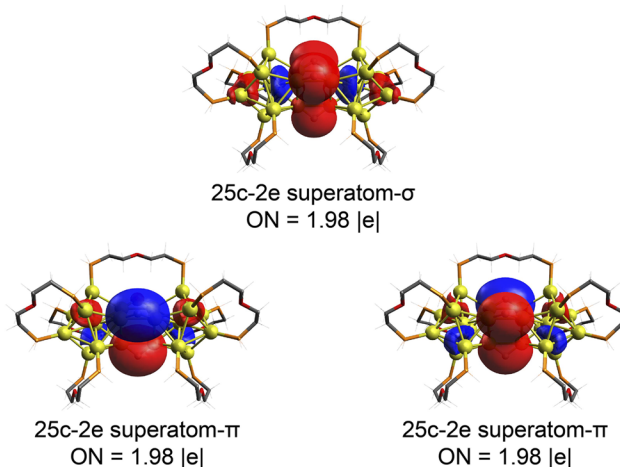

FIG. 7. The superatom–superatom triple bond revealed from AdNDP analyses for model 1 of the $[Au_{22}H_3(dppee)_7]^{3+}$ hydride nanocluster. ON = occupation number. The full AdNDP results are shown in Fig. S14.

electronic structure for the $[Au_{22}H_3(dppee)_7]^{3+}$ trihydride nanocluster, in agreement with its high stability (Fig. 2).

IV. CONCLUSIONS

In conclusion, we report the synthesis and characterization of a new and highly stable diphosphine-protected gold trihydride nanocluster, $[Au_{22}H_3(dppee)_7]^{3+}$. High purity samples can be obtained with reasonable yields, and they are stable under ambient conditions. The properties of the trihydride nanocluster are characterized using different spectroscopic methods, augmented with theoretical calculations. Both experimental evidence and theoretical evidence suggested that the new $[Au_{22}H_3(dppee)_7]^{3+}$ cluster has a similar structure as the $[Au_{22}H_4(L^8)_6]^{2+}$ cluster reported recently. The Au_{22} core in $[Au_{22}H_3(dppee)_7]^{3+}$ is composed of two Au_{11} units bonded via six uncoordinated gold atoms, where the three hydrogens are located in the bridging positions. Each Au_{11} unit can be viewed as a trivalent eight-electron superatom, forming a superatom–superatom triple bond ($Au_{11} \equiv Au_{11}$) in the $[Au_{22}H_3(dppee)_7]^{3+}$ nanocluster. The trihydride cluster is found to undergo rapid isotope exchange reactions with $NaBD_4$, suggesting that it could be a good catalytic model for investigating the mechanisms of hydrogenation reactions.

SUPPLEMENTARY MATERIAL

See the supplementary material for Figs. S1–S14 and Table S1.

ACKNOWLEDGMENTS

DATA AVAILABILITY

The data that support the findings of this study are available from the corresponding author upon reasonable request.

REFERENCES

[1] M. Haruta, Catal. Today **36**, 153–166 (1997).
[2] M. Valden, X. Lai, and D. W. Goodman, Science **281**, 1647–1650 (1998).
[3] P. Pyykkö, Chem. Soc. Rev. **37**, 1967–1997 (2008).
[4] H. Häkkinen, Chem. Soc. Rev. **37**, 1847–1859 (2008).
[5] D. Schooss, P. Weis, O. Hampe, and M. M. Kappes, Philos. Trans. R. Soc., A **368**, 1211–1243 (2010).
[6] L.-M. Wang and L.-S. Wang, Nanoscale **4**, 4038–4053 (2012).
[7] A. P. Woodham and A. Fielicke, Struct. Bonding **161**, 243–278 (2014).
[8] A. Sanchez, S. Abbet, U. Heiz, W.-D. Schneider, H. Häkkinen, R. N. Barnett, and U. Landman, J. Phys. Chem. A **103**, 9573–9578 (1999).
[9] W. T. Wallace and R. L. Whetten, J. Am. Chem. Soc. **124**, 7499–7505 (2002).
[10] S. M. Lang and T. M. Bernhardt, Phys. Chem. Chem. Phys. **14**, 9255–9269 (2012).
[11] J. Li, X. Li, H. J. Zhai, and L. S. Wang, Science **299**, 864–867 (2003).
[12] X. Xing, B. Yoon, U. Landman, and J. H. Parks, Phys. Rev. B **74**, 165423 (2006).
[13] A. Lechtken, C. Neiss, J. Stairs, and D. Schooss, J. Chem. Phys. **129**, 154304 (2008).

[14] P. Gruene, D. M. Rayner, B. Redlich, A. F. G. van der Meer, J. T. Lyon, G. Meijer, and A. Fielicke, Science **321**, 674–676 (2008).
[15] Z. W. Wang and R. E. Palmer, Nanoscale **4**, 4947–4949 (2012).
[16] Z. Li, H.-Y. T. Chen, K. Schouteden, T. Picot, T.-W. Liao, A. Seliverstov, C. Van Haesendonck, G. Pacchioni, E. Janssens, and P. Lievens, Sci. Adv. **6**, eaay4289 (2020).
[17] L. Molina and B. Hammer, J. Catal. **233**, 399–404 (2005).
[18] C. Yu, W. Harbich, L. Sementa, L. Ghiringhelli, E. Aprà, M. Stener, A. Fortunelli, and H. Brune, J. Chem. Phys. **147**, 074301 (2017).
[19] L. Yan, J. Xu, F. Wang, and S. Meng, J. Phys. Chem. Lett. **9**, 63–69 (2018).
[20] H.-F. Zhang, M. Stender, R. Zhang, C. Wang, J. Li, and L.-S. Wang, J. Phys. Chem. B **108**, 12259–12263 (2004).
[21] Q.-F. Zhang, X. Chen, and L.-S. Wang, Acc. Chem. Res. **51**, 2159–2168 (2018).
[22] M. F. Bertino, Z.-M. Sun, R. Zhang, and L.-S. Wang, J. Phys. Chem. B **110**, 21416–21418 (2006).
[23] J. Chen, Q.-F. Zhang, T. A. Bonaccorso, P. G. Williard, and L.-S. Wang, J. Am. Chem. Soc. **136**, 92–95 (2014).
[24] Q.-F. Zhang, P. G. Williard, and L.-S. Wang, Small **12**, 2518–2525 (2016).
[25] Z. Wu, G. Hu, D.-e. Jiang, D. R. Mullins, Q.-F. Zhang, L. F. Allard, Jr., L.-S. Wang, and S. H. Overbury, Nano Lett. **16**, 6560–6567 (2016).
[26] Z. Wu, D. R. Mullins, L. F. Allard Jr, Q. F. Zhang, and L. S. Wang, Chin. Chem. Lett. **29**, 795–799 (2018).
[27] F. Li and Q. Tang, Phys. Chem. Chem. Phys. **21**, 20144–20150 (2019).
[28] G. Hu, Z. Wu, and D.-e. Jiang, J. Mater. Chem. A **6**, 7532–7537 (2018).
[29] J. Dong, Z. H. Gao, Q. F. Zhang, and L. S. Wang, Angew. Chem., Int. Ed. **60**, 2424–2430 (2021).
[30] C. Donnerer, T. Scheler, and E. Gregoryanz, J. Chem. Phys. **138**, 134507 (2013).
[31] M. Rahm, R. Hoffmann, and N. W. Ashcroft, J. Am. Chem. Soc. **139**, 8740–8751 (2017).
[32] L. Andrews and X. Wang, J. Am. Chem. Soc. **125**, 11751–11760 (2003).
[33] S. Buckart, G. Ganteför, Y. D. Kim, and P. Jena, J. Am. Chem. Soc. **125**, 14205–14209 (2003).
[34] H.-T. Liu, Y.-L. Wang, X.-G. Xiong, P. D. Dau, Z. A. Piazza, D.-L. Huang, C.-Q. Xu, J. Li, and L.-S. Wang, Chem. Sci. **3**, 3286–3295 (2012).
[35] H.-J. Zhai, B. Kiran, and L.-S. Wang, J. Chem. Phys. **121**, 8231–8236 (2004).
[36] M. M. Giangregorio, M. Losurdo, G. V. Bianco, A. Operamolla, E. Dilonardo, A. Sacchetti, P. Capezzuto, F. Babudri, and G. Bruno, J. Phys. Chem. C **115**, 19520–19528 (2011).
[37] M. Conte, H. Miyamura, S. Kobayashi, and V. Chechik, J. Am. Chem. Soc. **131**, 7189–7196 (2009).
[38] I. P. Silverwood, S. M. Rogers, S. K. Callear, S. F. Parker, and C. R. A. Catlow, Chem. Commun. **52**, 533–536 (2016).
[39] D. Sil, C. Lane, E. Glor, K. D. Gilroy, S. Sylla, B. Barbiellini, R. Markiewicz, M. Hajfathalian, S. Neretina, A. Bansil, Z. Fakhraai, and E. Borguet, ChemistrySelect **4**, 4287–4292 (2019).
[40] P. D. Jadzinsky, G. Calero, C. J. Ackerson, D. A. Bushnell, and R. D. Kornberg, Science **318**, 430–433 (2007).
[41] P. Maity, S. Xie, M. Yamauchi, and T. Tsukuda, Nanoscale **4**, 4027–4037 (2012).
[42] K. Konishi, Struct. Bonding **161**, 49–86 (2014).
[43] R. Jin, C. Zeng, M. Zhou, and Y. Chen, Chem. Rev. **116**, 10346–10413 (2016).
[44] W. Kurashige, Y. Niihori, S. Sharma, and Y. Negishi, Coord. Chem. Rev. **320–321**, 238–250 (2016).
[45] I. Chakraborty and T. Pradeep, Chem. Rev. **117**, 8208–8271 (2017).
[46] Q. Yao, T. Chen, X. Yuan, and J. Xie, Acc. Chem. Res. **51**, 1338–1348 (2018).
[47] Z. Lei, X.-K. Wan, S.-F. Yuan, Z.-J. Guan, and Q.-M. Wang, Acc. Chem. Res. **51**, 2465–2474 (2018).
[48] J. Yan, B. K. Teo, and N. Zheng, Acc. Chem. Res. **51**, 3084–3093 (2018).
[49] S. Takano, H. Hirai, S. Muramatsu, and T. Tsukuda, J. Am. Chem. Soc. **140**, 8380–8383 (2018).
[50] A. Cirri, H. M. Hernández, and C. J. Johnson, Chem. Commun. **56**, 1283–1285 (2020).
[51] M. A. Hewitt, H. Hernández, and G. E. Johnson, J. Phys. Chem. C **124**, 3396–3402 (2020).

[52] M. A. Hewitt, H. Hernández, and G. E. Johnson, J. Am. Soc. Mass Spectrom. **32**, 237–246 (2021).

[53] M. R. Ligare, K. A. Morrison, M. A. Hewitt, J. U. Reveles, N. Govind, H. Hernandez, E. S. Baker, B. H. Clowers, J. Laskin, and G. E. Johnson, J. Phys. Chem. Lett. **12**, 2502–2508 (2021).

[54] S.-F. Yuan, J.-J. Li, Z.-J. Guan, Z. Lei, and Q.-M. Wang, Chem. Commun. **56**, 7037–7340 (2020).

[55] A. D. Becke, Phys. Rev. A **38**, 3098–3100 (1988).

[56] J. P. Perdew, K. Burke, and M. Ernzerhof, Phys. Rev. Lett. **77**, 3865–3868 (1996).

[57] C. Adamo and V. Barone, J. Chem. Phys. **110**, 6158–6170 (1999).

[58] T. Lu and F. Chen, J. Comput. Chem. **33**, 580–592 (2012).

[59] D. Y. Zubarev and A. I. Boldyrev, Phys. Chem. Chem. Phys. **10**, 5207–5217 (2008).

[60] M. J. Frisch, G. W. Trucks, H. B. Schlegel, G. E. Scuseria, M. A. Robb, J. R. Cheeseman, G. Scalmani, V. Barone, G. A. Petersson, H. Nakatsuji, X. Li, M. Caricato, A. Marenich, J. Bloino, B. G. Janesko, R. Gomperts, B. Mennucci, H. P. Hratchian, J. V. Ortiz, A. F. Izmaylov, J. L. Sonnenberg, D. Williams-Young, F. Ding, F. Lipparini, F. Egidi, J. Goings, B. Peng, A. Petrone, T. Henderson, D. Ranasinghe, V. G. Zakrzewski, J. Gao, N. Rega, G. Zheng, W. Liang, M. Hada, M. Ehara, K. Toyota, R. Fukuda, J. Hasegawa, M. Ishida, T. Nakajima, Y. Honda, O. Kitao, H. Nakai, T. Vreven, K. Throssell, J. A. Montgomery, Jr., J. E. Peralta, F. Ogliaro, M. Bearpark, J. J. Heyd, E. Brothers, K. N. Kudin, V. N. Staroverov, T. Keith, R. Kobayashi, J. Normand, K. Raghavachari, A. Rendell, J. C. Burant, S. S. Iyengar, J. Tomasi, M. Cossi, J. M. Millam, M. Klene, C. Adamo, R. Cammi, J. W. Ochterski, R. L. Martin, K. Morokuma, O. Farkas, J. B. Foresman, and D. J. Fox, Gaussian 09, Revision D.01, Gaussian, Inc., Wallingford, CT, 2013.

[61] L. C. McKenzie, T. O. Zaikova, and J. E. Hutchison, J. Am. Chem. Soc. **136**, 13426–13435 (2014).

[62] G. Hu, Q. Tang, D. Lee, Z. Wu, and D.-e. Jiang, Chem. Mater. **29**, 4840–4847 (2017).

[63] A. Muñoz-Castro, Phys. Chem. Chem. Phys. **22**, 1422–1426 (2020).